Brillouin scattering from off-axis acoustoelectric domains in CdS and ZnO

Ole Keller*
Physics Laboratory, The Royal Veterinary and Agricultural University, Copenhagen, Denmark
(Received 5 November 1973)

The time evolution of the angular phonon distribution in off-axis acoustoelectric domains has been investigated. In the weak-flux regime a single peak is observed, whereas complicated two-peak structures show up at certain frequencies in the strong-flux regime. The field dependence of the off-axis angle of maximum intensity, θ_{pmi}, agrees with theory in the linear region. In the nonlinear region oscillations superimposed on a "track-down" occur in the time development of θ_{pmi}. Anisotropy effects in acoustoelectric domains have been studied by measuring the domain tilt angle and the time evolution of the spatial acoustic energy density. It is shown that the branches of a V-formed domain contain different wave-vector distributions and that an incomplete regeneration effect causes a spatial splitting of the flux. In the 45° configuration phonon focusing is observed. We also present a calculation of the angular phonon bandwidth at $f = \tilde{f}_m$ based on the linear theory of anisotropic acoustic amplification. Using a simplified nonlinear model, the time development of the angle of maximum gain has been evaluated. The theory of acoustic-wave dispersion is outlined, and it is shown that the angular phonon focusing is appreciably enhanced for frequencies around $\tilde{f}_m$ if we account for the acoustoelectric angular dispersion.

I. INTRODUCTION

It is well known that the interaction of acoustic phonons with free charge carriers is responsible for the amplification of lattice vibrations from the thermal-equilibrium spectrum when the carrier drift velocity exceeds the sound velocity by the application of a sufficiently high electric field.[1-3] In strong piezoelectric semiconductors like ZnO and CdS the transfer of energy and momentum from the conduction electrons to elastic waves in the microwave region is caused by the piezoelectric coupling.[4] The acoustoelectrically amplified flux is usually found to be concentrated in domains formed at one electrode and propagating with a velocity close to the transverse velocity of sound in the direction of carrier drift.[5-10] The intense acoustic flux in the domains is restricted to contain phonons in a narrow cone along a favorable piezoelectrically active direction[11-15] and to a band of frequencies determined by the parameters of the material.[13,16-19] Acoustoelectric domains have been studied by various methods: electrical probing,[5,20] microwave emission,[21] transmission of microwave radiation,[7] recombination radiation,[22] high-electric-field[23] or strain-[24] induced birefringence, Brillouin scattering,[16,25] transmission and absorption of light near the intrinsic absorption edge,[26] and x-ray scattering.[27,28] Brillouin scattering and x-ray diffraction are the most powerful of these methods because they allow us to resolve the plane-wave components of the acoustic disturbance. So far, only a few x-ray-scattering experiments have been performed.[27,28] Many Brillouin-scattering investigations in ZnO and CdS concerning the time development of the frequency spectrum and the angular distribution in the so-called weak-[13,18] and strong-flux[12,14,16,25,29] regimes have been reported. However, most of these studies have been limited to the transverse configuration where the propagation vectors are confined to a cone around the direction of electron drift, which is perpendicular to the c axis. For small cone angles the flux evolution can be described by a one-dimensional model. If an appreciable amount of off-axis flux is present the lack of rotational symmetry about the current direction makes the analysis extremely complicated.

In the present work we have studied the domain propagation in the longitudinal configuration where the electric field is applied along the c axis of the crystal. In this case formation of acoustoelectric domains is due to buildup of polarized off-axis quasishear waves rather than longitudinal waves, because the phase velocity of longitudinal waves is around a factor of 2 higher than that of shear waves, and since the piezoelectric coupling vanishes for shear waves propagating parallel to c.[14,24] Although the acoustic flux, if surface effects are neglected, should exhibit complete rotational symmetry around the c axis in the longitudinal configuration, the investigations become involved because of the existence of pronounced anisotropy effects. On the other hand, measurements of the field and time dependence of the angular distribution of off-axis phonons with various frequencies and of domain tilt angles we believe will contribute essentially to the attainment of new aspects of traveling acoustoelectric domains.

In Sec. II we review the macroscopic linear theory of acoustic amplification[1] generalized to apply to waves propagating in an arbitrary crystallographic direction in a hexagonal crystal.[30] The directional dependence of the amplification coef-

ficient is discussed in the high-conductivity limit applicable to semiconducting materials, and the field dependence of the off-axis angle of maximum gain for the phase propagation, θ_{pm}, is calculated for ZnO and CdS. Using the theory of Klein[30] we have evaluated the angular phonon bandwidth at $f=\tilde{f}_m$ for various dc electric fields and by generalizing a simple nonlinear model by Gay and Hartnagel[31] the time evolution of θ_{pm} is calculated. The analysis of propagating acoustoelectric domains formed by off-axis quasishear waves involves a study of acoustic-wave dispersion arising from the presence of pure elastic,[14,24] piezoelectric, and dielectric anisotropy.[32] The influence of velocity dispersion on the domain propagation is normally negligible,[32] whereas the angular dispersion composed of a frequency-independent contribution from elastic anisotropy[14,24] and a frequency-dependent contribution from screened piezoelectric anisotropy[32,33] can produce a significant angular deviation between group and phase velocity. The treatment in Sec. II is valid in the weak-flux region. Although the complete process of domain growth and formation involves highly nonlinear interactions, it is found experimentally[34] that linear theory leaves its imprint on the final domain shape.

Section III contains a treatment of the theory of Brillouin scattering in optically anisotropic crystals. The polarization rotation of light scattered from the acoustic T_1, T_2, and L modes and the cutoff in the diffraction at high and low acoustic frequencies are examined. The anisotropic Bragg formulas are used to calculate the scattering geometry for acoustic waves having different frequencies and propagating in an arbitrary crystallographic direction. An expression for the intensity of the Brillouin-scattered light inside the crystal has been derived. Taking into account multiple internal reflections of the scattered light and the relation between the collection cone inside and outside the crystal enables us to determine the acoustic energy density per unit bandwidth in the domain in terms of the diffracted-light intensity.

Section IV covers the experimental results. The time and space development of the angular phonon distribution of different frequencies in the domain is examined. In the early stages of domain growth, a single peak is observed, whereas complicated two-peak structures show up at certain frequencies in the fully formed domain. The field dependence of the off-axis angle of maximum gain agrees qualitatively with the theory in the linear regime. In the nonlinear region oscillations superimposed on a "track-down" of the off-axis angle of maximum intensity occur. The influence of anisotropy effects on the acoustoelectric domain propagation has been investigated through measurements of domain tilt angles. In the strong-flux region the main contribution to the angular dispersion comes from the frequency-independent elastic anisotropy since the acoustic flux is dominated by frequencies below the frequency of maximum linear net gain. An experimental study of the frequency-dependent acoustoelectric angular dispersion supposed to exist in the weak-flux region has not been carried out.

In the longitudinal configuration the domain is V formed, whereas it has a straight shape in the so-called 45° configuration because of the existence of a pronounced energy focusing caused by the wave-dispersion effects. The two branches of a V-formed domain contain different wave-vector distributions. During the propagation of a V-formed domain an incomplete regeneration effect in the center of the domain often splits up the flux into two separate wave packets traveling near opposite crystal surfaces. The above observations indicate the existence of annular domains, an interesting possibility which should be investigated.

II. THEORY

A. Anisotropic acoustic amplification

The macroscopic linear theory of acoustoelectric coupling as derived by Hutson and White[1] and by Gurevich[35] is valid only when the applied electric field and the acoustic wave vector are parallel to a crystal axis of high symmetry. A modified small-signal theory which applies to the analysis of the off-axis acoustic flux generated when a sufficiently high electric field is applied along an arbitrary crystallographic direction has been obtained by Klein,[30] who takes into account the anisotropic dielectric, piezoelectric, and elastic properties of the semiconductor. The generalized expression for the amplitude amplification coefficient takes the usual form,

$$\alpha_e = \frac{K^2\tilde{\omega}_c}{2V_p}\left(\frac{\bar{\gamma}}{\bar{\gamma}^2+[(\tilde{\omega}_c/\omega)+(\omega/\tilde{\omega}_D)]^2}\right), \tag{1}$$

where $K^2 = K^2(\hat{\pi}, \hat{\kappa}_k) = \tilde{e}^2/(\tilde{c}\,\tilde{\epsilon})$ is the square of the electromechanical coupling constant, $\tilde{\omega}_c = (qn_0\kappa_{k,i} \times \mu_{ij}\kappa_{k,j})/\tilde{\epsilon}$ and $\tilde{\omega}_D = V_p^2/(\kappa_{k,i}D_{ij}\kappa_{k,j})$ are generalizations to the anisotropic case of the corresponding conductivity relaxation frequency and free-carrier diffusion frequency in the Hutson-White theory, $\bar{\gamma} = (\kappa_{k,i}V_{d,i})/V_p - 1 = (\kappa_{k,i}\mu_{ij}E_{0,j})/V_p - 1$ is the drift parameter, and $\hat{\pi}$ and $\hat{\kappa}_k = \vec{k}/k$ are unit vectors in the direction of polarization of the acoustic mode and along the acoustic wave vector ($\vec{k}$). c_{ijkl}, e_{ijk}, and ϵ_{ij} are the elastic, piezoelectric, and dielectric tensors, $\tilde{c} = \pi_i\kappa_{k,j}c_{ijkl}\pi_k\kappa_{k,l}$, $\tilde{\epsilon} = \kappa_{k,i}\epsilon_{ij}\kappa_{k,j}$, and $\tilde{e} = \kappa_{k,i}e_{ijk}\pi_j\kappa_{k,k}$. μ_{ij} and D_{ij} are tensors describing the anisotropic carrier mobility and diffusion. $\vec{V}_d$ is the carrier drift velocity and $\vec{V}_p(\hat{\pi}, \hat{\kappa}_k)$ the appropriate acoustic phase velocity. The above notation implies summation over repeated subscripts. In the longitudinal configuration the dc field is ap-

plied along the c axis so that the drift parameter reduces to

$$\tilde{\gamma} = \frac{V_d}{V_p(\theta_p)} \cos\theta_p - 1 \quad , \tag{2}$$

where θ_p is the angle between the acoustic wave vector and the optic axis. Note that when calculating the angular dependence of the acoustoelectric gain one must account for the anisotropy of the acoustic phase velocity. If we neglect nonelectronic losses the condition of obtaining amplification in a given direction is that $V_d \cos\theta_p / V_p(\theta_p) > 1$, which means that the component of the carrier (electron) drift velocity along the direction of acoustic-wave propagation must exceed the acoustic phase velocity in this direction. In the generalized theory the frequency of maximum linear gain $\tilde{\omega}_m = (\tilde{\omega}_c \tilde{\omega}_D)^{1/2}$ is an anisotropic quantity which varies as $\tilde{\omega}_m(\theta_p)/\tilde{\omega}_m(0) = [V_p(\theta_p)/V_p(0)][\epsilon(0)/\epsilon(\theta_p)]^{1/2}$. In ZnO and CdS the relative directional variation in $\tilde{\omega}_m$ is 10–20%. Introducing the approximation $\tilde{\gamma}^2 \ll 4\,\tilde{\omega}_c/\tilde{\omega}_D \lesssim (\tilde{\omega}_c/\omega + \omega/\tilde{\omega}_D)^2$, which is usually correct in the high-conductivity limit applicable to semiconducting materials, the expression for the amplification coefficient reduces to $\alpha_e \approx K^2(\theta_p)\,\tilde{\omega}_D \tilde{\gamma}/8 V_p(\theta_p)$ at $\omega = \tilde{\omega}_m$. Considering only the angular-dependent factors in α_e we obtain (assuming D_{ij} to be isotropic is a fair approximation in ZnO and CdS)

$$\alpha_e(\theta_p) \propto \frac{V_p(\theta_p)}{V_p(0)} K^2(\theta_p) \left(\frac{V_d}{V_p(0)} \frac{V_p(0)}{V_p(\theta_p)} \cos\theta_p - 1 \right) \quad . \tag{3}$$

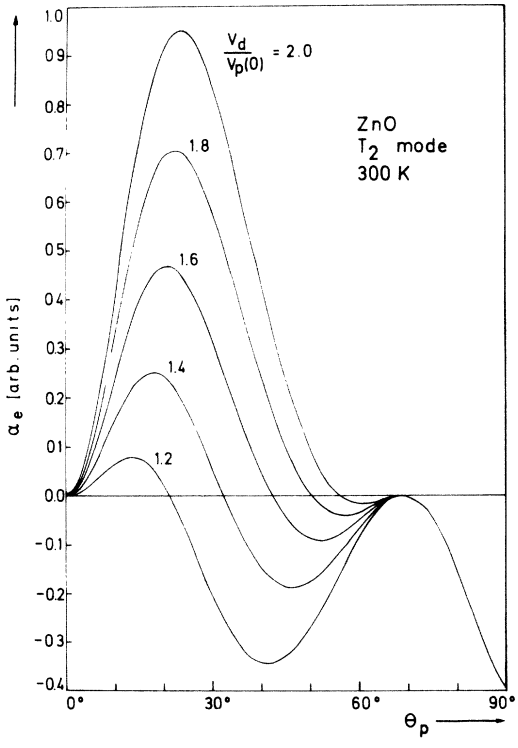

FIG. 1. Dependence of small-signal amplitude-amplification coefficient α_e (in arbitrary units) on propagation direction (θ_p) of acoustic mode relative to the c axis with the normalized drift velocity as a parameter.

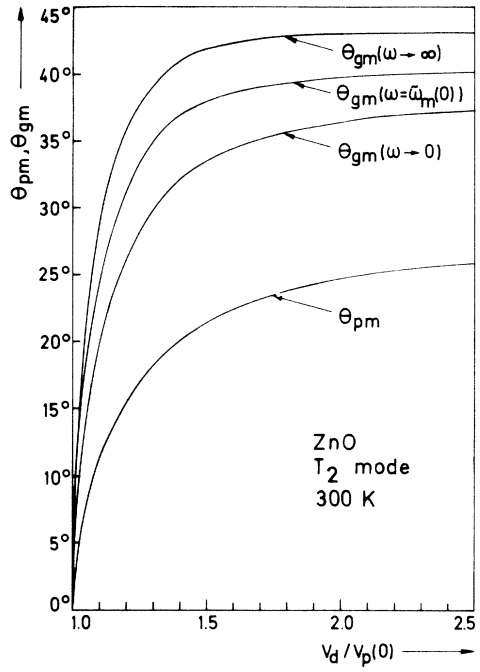

FIG. 2. Off-axis angle of maximum gain for the phase propagation (θ_{pm}), and for the group propagation (θ_{gm}) at different frequencies (0, $\tilde{\omega}_m$, ∞) vs the normalized drift velocity.

In Fig. 1 is plotted the amplitude amplification coefficient (in arbitrary units) of the quasitransverse T_2 mode in ZnO as a function of the off-axis angle of phase propagation, with the normalized drift velocity $V_d/V_p(0)$ as a parameter.[36,37] As the electric field (and thus the electron drift velocity in the linear theory) increases more modes at larger angles from the c axis are amplified. At $\theta_p = 0°$, 68° one has $\alpha_e = 0$, independent of $V_d/V_p(0)$ because the electromechanical coupling constant vanishes in these directions. The angular dependence of the gain factor in CdS has been calculated by Klein[30] and by Moore *et al.*[24] The off-axis angle of maximum gain for the phase propagation (θ_{pm}) is a monotonic increasing function of the field strength (or the drift velocity) as shown in Fig. 2. For $V_d/V_p(0) \to 0$, $\theta_{pm} \to 0$, and in the high-field limit θ_{pm} saturates at the value where the function $K^2(\theta_p) \times \cos\theta_p$ has its maximum.

When the electric field coincides in direction with the c axis, the angular distribution of the emitted phonons is symmetric with respect to the field

direction and a cross section of the gain cone containing the c axis consists of two (symmetric) lobes. Therefore, the angular selectivity of the amplification process can be examined by calculating the angular bandwidth $\delta\theta_p$ (i.e., the angle between the half-intensity directions in one of the lobes). The growth in time and space of the acoustic energy density per unit volume in $\vec{q}$ space $W_{\vec{q}}$ is given by

$$\vec{V}_g(\theta_p+\Delta)\cdot\vec{\nabla}\,W_{\vec{q}}+\frac{\partial W_{\vec{q}}}{\partial t}=W_{\vec{q}}[\beta_e(\theta_p)-\alpha_L(\theta_p)]\,V_g(\theta_p+\Delta)\times\cos\Delta+W^{\rm th}[\beta_{e0}(\theta_p)+\alpha_L(\theta_p)]\,V_g(\theta_p+\Delta)\cos\Delta\quad,\tag{4}$$

where $W^{\rm th}=k_BT/(2\pi)^3$ is the thermal energy density corresponding to a single polarization, $\beta_e=2\alpha_e$ is the acoustoelectric power-gain coefficient, and α_L is the nonelectronic lattice attenuation coefficient. β_{e0} is introduced through the equation $\beta_e=\beta_{e0}\tilde{\gamma}$. $\vec{V}_g$ is the group velocity of the acoustic modes ($\vec{q}\mid\vec{q}+d\vec{q}$) under consideration, and $\Delta=\Delta(\theta_p)$ is the angular deviation of the group velocity from the phase velocity.[32] A careful treatment of the acoustic dispersion (see Sec. II B) is important since it is the group velocity $\vec{V}_g(\theta_p+\Delta)$ which provides the propagation direction of the energy, whereas it is the phase velocity $\vec{V}_p(\theta_p)$ which determines the amplification rate. The second term on the right-hand side of Eq. (4) is necessary to guarantee that the net energy exchange between the electron gas and the acoustic flux vanishes in thermal equilibrium. Integration of Eq. (4) yields

$$W_{\vec{q}}=W^{\rm th}\left[\left(1+\frac{\beta_{e0}+\alpha_L}{\beta_n}\right)e^{(\beta_e-\alpha_L)\cos\Delta V_g t}-\frac{\beta_{e0}+\alpha_L}{\beta_n}\right]\quad,\tag{5}$$

where $\beta_n=\beta_e-\alpha_L$ is the net acoustic power-gain coefficient. The factor in front of the exponential is of the order of unity for the frequencies of interest if $\beta_n=\beta_e-\alpha_L$ is not too close to zero.[37] Assuming that the flux has been amplified to a level well above the thermal background, i.e., $W_{\vec{q}}\gg W^{\rm th}$ the angular bandwidth $\delta\theta_p(t)=\theta_{p,1/2}-\theta_{p,-1/2}$ can be calculated from

$$[\beta_e(\theta_{\rm pm})-\alpha_L(\theta_{\rm pm})]\,V_g(\theta_{\rm pm}+\Delta(\theta_{\rm pm}))\cos\Delta(\theta_{\rm pm})-[\beta_e(\theta_p)-\alpha_L(\theta_p)]\,V_g(\theta_p+\Delta(\theta_p))\cos\Delta(\theta_p)=\ln 2/t\quad,\tag{6}$$

which has the solutions $\theta_p=\theta_{p,1/2}$, $\theta_{p,-1/2}$.

The results of a numerical calculation of the time dependence of the angular bandwidth in ZnO are shown in Fig. 3. $\delta\theta_p(t)$ depends on the acoustic frequency and is drawn only for $\omega=\tilde{\omega}_m(\theta_{\rm pm})$. As an approximation, which can be justified experimentally,[38,39] the directional dependence of α_L has been neglected. For small t, $\delta\theta_p$ is constant, indicating that all modes having net gain are within the angular bandwidth. After a certain time, which depends strongly on the normalized drift velocity $V_d/V_p(0)$, the bandwidth decreases. Note that most of the collapse in $\delta\theta_p$ occurs during the first 10 nsec of the decay. From the inset of Fig. 3 it appears that in the first stages of the bandwidth shrinkage the off-axis angle of maximum gain does not coincide with the mean value $\frac{1}{2}(\theta_{p,1/2}+\theta_{p,-1/2})$. Above the angular bandwidth has been calculated assuming a constant drift velocity. This holds only during the incubation time t_i. Modifying the approximate expression for t_i from the one-dimensional model[40] to the general case we obtain, by using the continuity equation and the Weinreich relation and by taking anisotropy effects into account,

$$t_i\approx\ln\left(\frac{J_s\{[V_d/V_p(0)]-1\}}{e[\beta_e(\theta_{\rm pm})+\beta_{e0}(\theta_{\rm pm})]\,\mu W_0\cos[\theta_{\rm pm}+\Delta(\theta_{\rm pm})]\cos\Delta(\theta_{\rm pm})}\right)\Big/\beta_n(\theta_{\rm pm})\,V_g(\theta_{\rm pm}+\Delta(\theta_{\rm pm}))\cos\Delta(\theta_{\rm pm})\quad,\tag{7}$$

where $J_s=qn_0V_p(0)$ is the saturated current density and e is the base of the ln function. The thermal-equilibrium acoustic energy density is approximated by the formula $W_0=(2\pi\langle V_p\rangle)^{-3}\tilde{\omega}_m^2\Delta\tilde{\omega}k_BT\Omega$, $\Delta\tilde{\omega}\approx\tilde{\omega}_m$ being the frequency range and Ω the solid angle in which the acoustic amplification takes

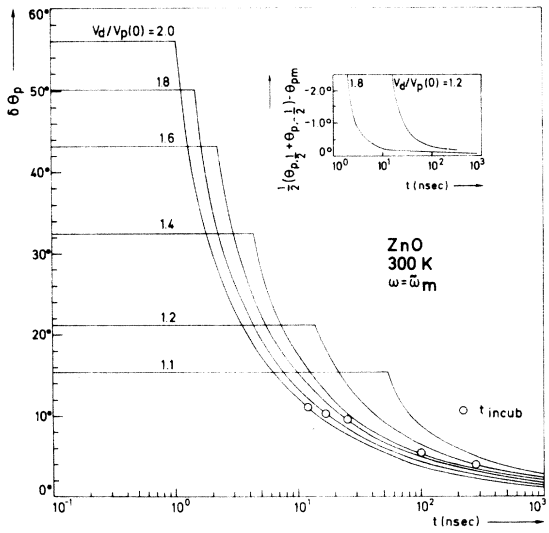

FIG. 3. Time dependence of the angular bandwidth ($\delta\theta_p$) at $\omega=\tilde{\omega}_m$ calculated on basis of linear theory for different normalized drift velocities. The incubation time is indicated in the figure. The insert shows the asymmetry in the bandwidth shrinkage.

place. $\langle V_p \rangle$ is the average value of V_p within Ω. Note that at $\omega = \tilde{\omega}_m(\theta_{pm})$ $V_g(\theta_p + \Delta)\cos\Delta \approx V_{p0}(\theta_p)(1 + K^2(\theta_p)/2)$.[32]

It is seen from Fig. 3 that most of the shrinkage in $\delta\theta_p$ takes place during the incubation time and thus within the limits of the linear theory.

As the acoustic flux becomes very intense the free carrier drift velocity decreases to a level close to the shear-wave phase velocity.[2] According to Fig. 2 this drop in the drift velocity is accompanied by a "track-down" in the off-axis angle of maximum gain for the phase (θ_{pm}). A simple single-mode analysis by Gay and Hartnagel[31] based on the power and momentum transfer from the electrons to the acoustic wave gives the time dependence of the drift parameter $\gamma_t \equiv \gamma(t)$ in the one-dimensional case. Generalizing their treatment to apply to off-axis acoustic waves the time dependence of the drift parameter γ_t can be obtained by solving the equation

$$Z(\theta_{pm})\frac{d}{dt}[\gamma_t - \gamma_L(\theta_{pm})] + \left(1 + Z(\theta_{pm})[\gamma_0(\theta_{pm}) - \gamma_L(\theta_{pm})]\, V_g(\theta_{pm} + \Delta_{pm})\beta_{e0}(\theta_{pm})\cos\Delta_{pm} + \frac{dZ(\theta_{pm})}{dt}\right)[\gamma_t - \gamma_L(\theta_{pm})]$$

$$= Z(\theta_{pm})\, V_g(\theta_{pm} + \Delta_{pm})\beta_{e0}(\theta_{pm})\cos\Delta_{pm}[\gamma_t - \gamma_L(\theta_{pm})]^2 + \frac{d}{dt}\{Z(\theta_{pm})[\gamma_0(\theta_{pm}) - \gamma_L(\theta_{pm})]\} \quad , \tag{8}$$

where

$$Z = \frac{l}{n_0 \rho \mu^2}\, V_p(\theta_{pm})\frac{\cos(\theta_{pm} + \Delta_{pm})}{\cos\theta_{pm}} \quad , \quad \gamma_L = \frac{\alpha_L}{\beta_{e0}(\theta_{pm})} \quad ,$$

and $\gamma_0 = \gamma_t(t = 0)$. l is the length of the crystal. Neglecting the time dependence of θ_{pm} in the slowly varying functions Z, γ_L, V_g, β_{e0}, and $\Delta_{pm} \equiv \Delta(\theta_{pm})$ the solution of Eq. (8) is

$$\gamma_t = \gamma_L + \frac{(\gamma_0 - \gamma_L)[1 + Z(\gamma_0 - \gamma_L)]}{Z(\gamma_0 - \gamma_L) + \exp\{[1 + Z(\gamma_0 - \gamma_L)/Z]\, V_g \beta_{e0} t \cos\Delta_{pm}\}} \quad . \tag{9}$$

Using $V_d(t) = (1 + \gamma_t)\, V_p(\theta_{pm}(t))/\cos\theta_{pm}(t)$ and the results shown in Fig. 2, $\theta_{pm} = \theta_{pm}(t)$ is obtained by an iteration procedure. Replacing $\theta_{pm}(0)$ by $\theta_{pm}(t)$ in Eq. (9) the time dependence of γ_t is practically unchanged, so that the obtained solution $\theta_{pm} = \theta_{pm}(t)$ is justified. For a ZnO crystal of length $l = 10$ mm and mobility $\mu = 150$ cm^2/V sec the "track-down" in θ_{pm} is shown in Fig. 4. As expected, the magnitude of the drop depends on the initial field strength. Close to the threshold field, i.e., for $V_d(t = 0)/V_p(\theta_p = 0) = 1.2$, $\theta_{pm}(t \to \infty) - \theta_{pm}(t = 0) \approx 6° - 7°$, whereas $V_d(t = 0)/V_p(\theta_p = 0) = 2.0$ yields $\theta_{pm}(t \to \infty) - \theta_{pm}(t = 0) \approx 16° - 17°$. The decay time of θ_{pm} is about 10–30 nsec and decreases slightly with increasing initial drift velocity. The saturation level $\theta_{pm}(t \to \infty)$ is determined by the condition that the nonelectronic losses just balance the electronic amplification. Consequently, $\theta_{pm}(t \to \infty)$ becomes a function of the acoustic frequency and of the resistivity.

Also, the off-axis angle of maximum intensity for the phase θ_{pmi} decreases as a function of time. However, the time constant involved in the decay of θ_{pm} must be less than that of θ_{pmi} since θ_{pmi} is determined by the amount of acoustic flux accumulated in different crystallographic direction, whereas θ_{pm} is determined by the instantaneous drift velocity.

B. Dispersion effects

Considering a disturbance, made up of the collection of plane acoustic waves of the same polarization type which have their propagation vectors in

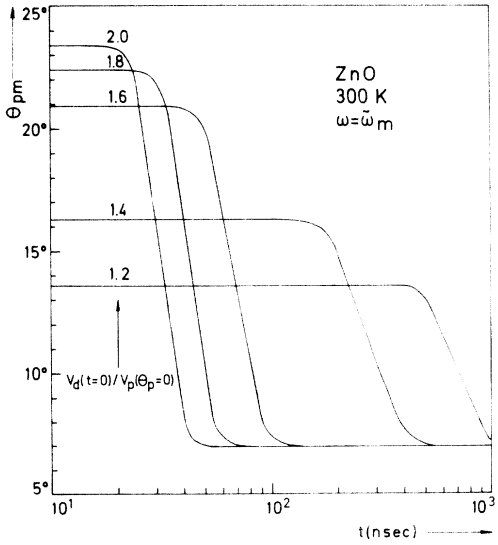

FIG. 4. Off-axis angle of maximum gain for the phase propagation (θ_{pm}) at $\omega = \tilde{\omega}_m$ as a function of time with the normalized drift velocity as a parameter.

a small volume element $d\vec{k}$ around an arbitrary wave vector $\vec{k}$, the group velocity $\vec{V}_g$ is determined by

$$\vec{V}_g = \vec{\nabla}_{\vec{k}}[k\, V_p(\vec{k})] \quad , \tag{10}$$

where $V_p(\vec{k})$ is the magnitude of the phase velocity corresponding to the selected $\vec{k}$. According to Eq. (10), acoustic waves propagating in a general crystallographic direction are normally subjected to velocity dispersion and angular dispersion.[32]

In the macroscopic small-signal theory of acoustic amplification the wave dispersion originates in elastic[14,24] and acoustoelectric anisotropy.[32,33] Writing the phase velocity in the form

$$V_p = V_{p0}(1+\chi) \quad , \tag{11}$$

where

$$\chi = \frac{K^2}{2}\left(1 - \frac{(\bar{\omega}_c/\omega)[(\bar{\omega}_c/\omega)+(\omega/\bar{\omega}_D)]}{\bar{\gamma}^2+[(\bar{\omega}_c/\omega)+(\omega/\bar{\omega}_D)]^2}\right) \quad , \tag{12}$$

the dispersion effects arising from the simultaneous presence of piezoelectricity and conductivity are contained in the quantity χ.

Confirming the treatment to hexagonal crystals we obtain for the group velocity, using Eqs. (10)–(12),

$$\vec{V}_g = V_p\hat{\kappa}_k + \hat{\kappa}_k\, k\, V_{p0}\frac{\partial\chi}{\partial k} + \hat{\kappa}_\theta(1+\chi)\frac{\partial V_{p0}}{\partial\theta_p} + \hat{\kappa}_\theta V_{p0}\frac{\partial\chi}{\partial\theta_p} \quad , \tag{13}$$

where $\hat{\kappa}_k$ and $\hat{\kappa}_\theta$ are unit vectors parallel and perpendicular to $\vec{k}$ in the plane defined by the c axis and the acoustic wave vector.

The frequency-dependent acoustoelectric velocity dispersion $\hat{\kappa}_k k V_{p0}(\partial\chi/\partial k)$ can only be of the order of K^2 and has been discussed in detail in Ref. 32. For acoustic waves with frequencies below or in the microwave region the purely elastic velocity dispersion is negligible.[41]

In connection with off-axis domain propagation the pronounced angular dispersion plays an important role. Expressing it in terms of the angular deviation Δ of the ray from the wave normal one finds[32,42]

$$\Delta = \arctan\left[\left(\frac{\partial\chi}{\partial\theta_p} + (1+\chi)\frac{\partial \ln V_{p0}}{\partial\theta_p}\right)\Big/\left(1+\chi+\omega\frac{\partial\chi}{\partial\omega}\right)\right] . \tag{14}$$

In the high-conductivity limit applicable to semiconducting materials, $\bar{\gamma}^2 \ll 4\,\bar{\omega}_c/\bar{\omega}_D$, so that the angular dispersion depends only on the normalized phonon frequency $\omega/\bar{\omega}_m$. For $\omega \to 0$, the acoustoelectric angular dispersion vanishes since the free carriers can redistribute themselves quickly enough to cancel the piezoelectric field. Thus, we are left with the frequency-dependent elastic angular dispersion, $\Delta_0 = \arctan(\partial \ln V_{p0}/\partial\theta_p)$. For $\omega \to \infty$, the angular dispersion approaches the piezoelectrically stiffened angular dispersion, $\Delta_s = \arctan\{\partial \ln V_{p0}/\partial\theta_p + [K/(1+\frac{1}{2}K^2)]\,\partial K/\partial\theta_p\}$. In directions where $K=0$ or K has a maximum $\Delta_s = \Delta_0$.

In Fig. 5 the deviation Δ is plotted as a function of θ_p for the acoustoelectrically active quasitransverse mode (T_2) in ZnO for three different acoustic frequencies. Note the pronounced frequency dependence of the acoustoelectric angular dispersion and its considerable magnitude. For $\theta_p = 0°$, $68°$ ($K=0$), and for $\theta_p = 90°$ ($K = K_{max}$, direction of high symmetry) the dispersion is independent of ω. In ZnO (and CdS) the dispersion curves for intermediate frequencies lie for almost every θ_p somewhere in between the high- and low-frequency limit which explains that $\Delta \approx \Delta_0 = \Delta_s$ for $\theta_p \approx 33°$ ($K \approx K_{max}$). For increasing ω, the off-axis angles of maximum dispersion are shifted towards lower values together with the angle for which $\Delta = 0$.

Angular focusing of energy, which is important for off-axis domain propagation, appears because of the decrease in Δ with increasing θ_p.[14,32–34,42] The strength of the angular focusing is obtained by calculating the angular distribution of group-velocity vectors associated with a uniform distribution of wave vectors in the interval $0° \le \theta_p \le 90°$.[42] In Fig. 6 the number of group-velocity vectors lying within intervals of $0.5°$ in θ_g associated with wave vectors taken at $0.05°$ interval in θ_p is plotted for different frequencies, given relative to $\bar{\omega}_m$ ($\theta_p = 0°$). Only part of the spectrum showing energy enhancement above the average value is drawn. Drastic changes in the spectrum are observed with

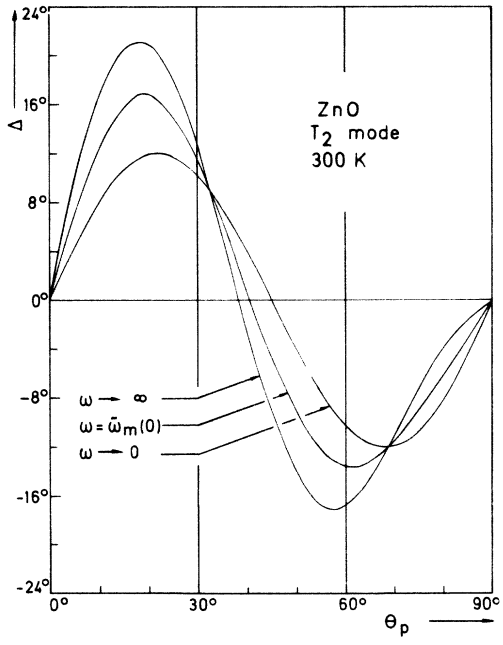

FIG. 5. Total angular dispersion (Δ) of the quasitransverse mode (T_2) plotted for different frequencies as a function of θ_p.

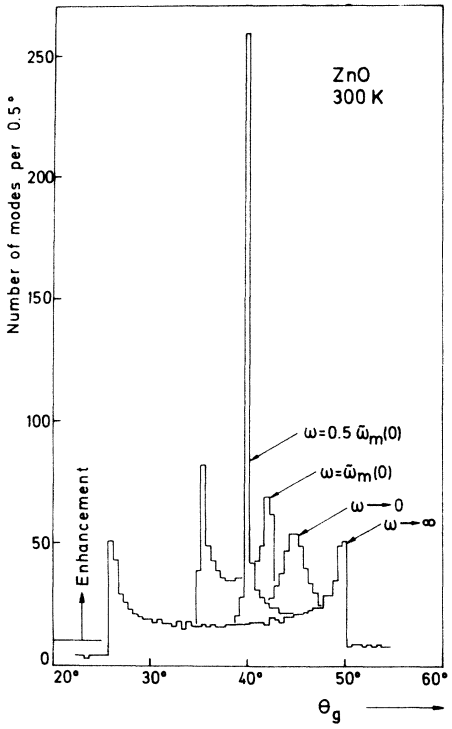

FIG. 6. Number of group-velocity vectors, associated with a uniform wave-vector distribution of density 20 modes/deg, lying within intervals of 0.5° in θ_g plotted for different phonon frequencies.

increasing ω. For low frequencies a single broad peak is found. At $\omega/\tilde{\omega}_m(0) = 0.5$ the focusing is so pronounced that 14.4% of the modes are focused in the region $40.0° \leq \theta_g < 40.5°$. As ω exceeds $\tilde{\omega}_m(0)$ the spectrum depresses at the center and steep jumps occur at the boundaries. Note also the downshift in peak position with increasing ω, and the antifocusing in the directions $\theta_p = 0, \frac{1}{2}\pi$.

A quantitative calculation of the angular dispersion effects of the T_2 mode in CdS is given in Refs. 32 and 42. Here we only emphasize that, although the elastic anisotropy dominates the angular dispersion, the energy focusing is still very sensitive to variations in the acoustic frequency. The intensity within a 0.5° interval in θ_g has an absolute maximum for $\omega/\tilde{\omega}_m(0) = 0.68$; thus 24.3% of the modes is focused in the interval $43.5° \leq \theta_g < 44.0°$.

To obtain the time-dependent angular energy distribution associated with an acoustoelectrically amplified portion of the thermal background flux one must weight the uniform distribution in accordance with the wave-vector distribution generated by the anisotropic amplification coefficient [Eq. (1)], add the frequency spectra scaled with the Debye factor ω^2, and introduce a cutoff frequency because of the nonelectronic lattice attenuation.[38,39]

III. ANISOTROPIC BRILLOUIN SCATTERING

A. Scattering geometry

Brillouin scattering can be considered in a particle picture as a phonon-photon interaction.[37,43] Let $\vec{k}_i$, $\vec{k}_d$, and $\vec{K}$ be the wave vectors in the medium of the incident photon, diffracted photon, and the acoustic phonon. If we ignore higher-order diffraction processes which correspond to a coherent sum of more than one three-particle scattering process, the conservation of pseudomomentum in the interaction can be expressed in the form

$$\vec{k}_i \pm \vec{K} = \vec{k}_d \quad . \tag{15}$$

The condition that energy must be conserved in the scattering process may be written

$$\omega_i \pm \Omega = \omega_d \quad , \tag{16}$$

where ω_i, ω_d, and Ω are the angular frequencies of the incident and scattered photon and the acoustic phonon. If a phonon is created in the collision event (minus sign), the frequency of the scattered light will be less than that of the incident beam, producing the so-called Stokes component, whereas, if a phonon is annihilated in the process (plus sign) the scattered light has a higher frequency, the anti-Stokes component.

Brillouin scattering provides a direct way of resolving the frequency and wave-vector components of the amplified acoustic flux. In the present work we shall limit our discussion to the scattering geometry shown in Fig. 7. It is assumed that the acoustic phonon propagates at a certain angle θ_p with respect to the optic axis (c) of the hexagonal crystal, and that the light wave vectors ($\vec{k}_i$, $\vec{k}_d$) are confined to the plane defined by the c axis and the acoustic wave vector ($\vec{K}$).

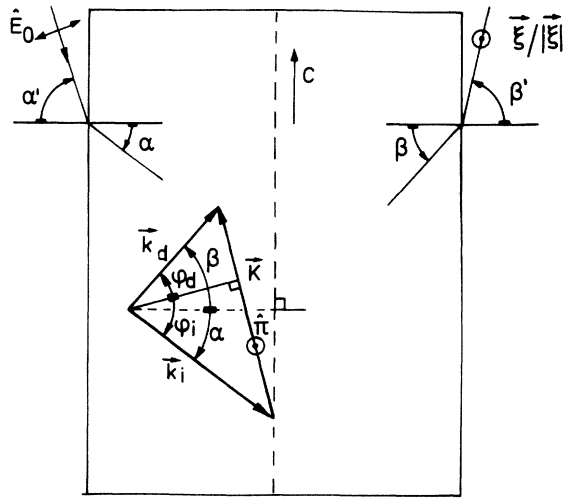

FIG. 7. Brillouin-scattering configuration used for diffraction from an off-axis inactive mode (T_1).

For microwave acoustic phonons one has $\Omega \ll \omega_i$, so that $\omega_i \approx \omega_d$. Thus the energy-conservation condition becomes $k_i/n_i \approx k_d/n_d$, where n_i and n_d are the refractive indices of the incident and scattered light. Using this relation, the quasi-momentum-conservation, Eq. (15), and the phonon dispersion relation, $K(\theta_p) = 2\pi f/V_p(\theta_p)$, we obtain the anisotropic Bragg equations corresponding to the anti-Stokes process,

$$\sin(\alpha + \theta_p) = \frac{\lambda_0}{2n_i(\alpha)\, V_p(\theta_p)} \left(f + \frac{V_p^2(\theta_p)}{f\lambda_0^2} \left[n_i^2(\alpha) - n_d^2(\beta) \right] \right) \tag{17}$$

and

$$\sin(\beta - \theta_p) = \frac{\lambda_0}{2n_d(\beta)\, V_p(\theta_p)} \left(f - \frac{V_p^2(\theta_p)}{f\lambda_0^2} \left[n_i^2(\alpha) - n_d^2(\beta) \right] \right), \tag{18}$$

where α and β are the angles of incidence and scattering inside the crystal and λ_0 is the wavelength of the incoming light in vacuum. For the Stokes process similar expressions can be derived. When the acoustic mode (f, θ_p) and λ_0 are given the above equations determine the scattering geometries for an absorption process.

The refractive indices n_i and n_d are in general different in optically anisotropic solids if the diffracted light has a polarization different from that of the incident light.[44] In this case the acoustic wave vector connects the endpoints of two wave vectors of light $(\vec{k}_i, \vec{k}_d)$ which belong to different shells of the refractive index surface. Also, if $\vec{k}_i$ and $\vec{k}_d$ belong to the same shell of the index surface, i.e., if the polarization of light is not changed by the diffraction, deviations from the isotropic Bragg geometry can occur.[37,45] In the geometry sketched in Fig. 7 a 90° rotation of the polarization of light is found upon scattering from the T_1 mode, whereas the T_2 and L modes do not change the plane of polarization.[37,46]

When the incident light is polarized in the scattering plane and the scattered beam is polarized perpendicular to this plane, due to scattering from the T_1 mode, we have $n_i = n_e n_o (n_o^2 \cos^2\alpha + n_e^2 \sin^2\alpha)^{-1/2}$ and $n_d = n_o$, n_e and n_o being the extraordinary and ordinary refractive indices. Substituting these expressions into Eqs. (17) and (18) the internal angles (α, β) can be worked out. The corresponding external angles (α', β') are obtained by using Snell's laws $\sin\alpha' = n_i(\alpha)\sin\alpha$ and $\sin\beta' = n_d(\beta)\sin\beta$. In the present case the anisotropic Bragg equations can be solved analytically only if the acoustic mode propagates either perpendicular ($\theta_p = \frac{1}{2}\pi$) or parallel ($\theta_p = 0$) to the c axis.[47] A numerical calculation of α' and β' as a function of the phonon frequency f with the off-axis angle θ_p as a parameter is shown for CdS in Fig. 8. Note that the angular dependence of the acoustic phase velocity is taken into account. A detailed analysis of Brillouin scattering from the T_1, T_2, and L modes as a function of f and θ in the scattering geometry shown in Fig. 7 will be published in a forthcoming paper.[46]

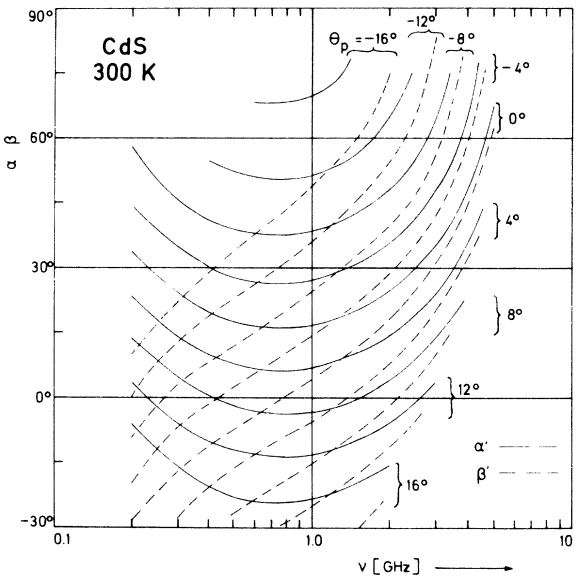

FIG. 8. Angle of incident light (α') and angle of diffracted light (β') outside the crystal as a function of the acoustic frequency for the scattering geometry shown in Fig. 7. The off-axis angle of phase propagation (θ_p) is a parameter.

In accordance with the anisotropic Bragg equations the acoustic phase velocity must be known in order to determine the frequency and propagation direction of the acoustic wave. If different acoustic polarizations are present (as is the case in a reflected domain)[34,38] a direct measurement of the frequency shift with a Fabry-Perot interferometer yields a substantial contribution to the mode identification.[34]

The first term on the right-hand side of the anisotropic Bragg equations is the usual isotropic term occurring when the momentum triangle is isosceles ($n_i = n_d$). The second term is present only in the anisotropic case. The two terms are equal in magnitude at the frequency $f' = V_p(|n_i^2 - n_d^2|)^{1/2}/\lambda_0$. For acoustic frequencies larger than f' the first term tends to dominate, while for frequencies less than f' the second term is more important. This shows that the optical anisotropy influences the scattering geometry especially at low frequencies. If the Brillouin scattering involves a polarization rotation there exists a lower critical acoustic frequency, $f_{\min} = |n_i - n_d|\, V_p/\lambda_0$, below which no diffraction can occur. Note that the interaction is collinear at $f = f_{\min}$. Furthermore, there always exists a frequency $f_{\max}$ above which no diffraction can take place. This frequency corresponds to a diffraction angle of 180°, and is given by $f_{\max} = (n_i + n_d)\, V_p/\lambda_0$. If total internal reflection

TABLE I. Comparison of the critical acoustic frequencies which occur in an anisotropic Bragg diffraction ($\theta_p = \frac{1}{2}\pi$, $\vec{k}_i \perp \vec{c}$). The frequencies are calculated for an optical wavelength of 6328 Å.

	ZnO	CdS
$f_{\min} = (n_e - n_o)V_p/\lambda_0$	74 MHz	44 MHz
$f' = (n_e^2 - n_o^2)V_p/\lambda_0$	1.1 GHz	0.8 GHz
$f_{\max} = 2nV_p/\lambda_0$	17.4 GHz	13.8 GHz

is taken into account $f_{\max}$ is reduced to $\sim 2V_p/\lambda_0$. $f_{\min}$ and f' vary considerably with the off-axis angle θ_p,[46] whereas $f_{\max}$ is almost independent of θ_p. As an example Table I shows the characteristic frequencies for the T_2 mode in ZnO and CdS in the case $\theta_p = \frac{1}{2}\pi$, $\vec{k}_i \perp \vec{c}$. For ZnO the following data were used: $V_p^{T2} = 2.74 \times 10^5$ cm/sec, $n_e = 2.011$, $n_o = 1.994$,[48] and for CdS: $V_p^{T2} = 1.77 \times 10^5$ cm/sec, $n_e = 2.468$, $n_o = 2.452$.[49]

The significant number of acoustic modes with frequencies below f' which ordinarily are present in an acoustoelectric domain[13,14,18] makes the above considerations essential for the interpretation of the Brillouin-scattering data.

B. Intensity of scattered light

The intensity of light scattered from an equilibrium thermal distribution of acoustic phonons into the solid angle $d\Omega$ is given by[46,50]

$$dI_{sc} = I_0 \frac{\pi^2 n_0^8}{\lambda_0^4} \sum_{\mu=1}^{3} \frac{|\vec{\xi}^{\mu}|^2}{2\rho V_{p,\mu}^2} \hbar\Omega_{\mu}(\vec{K}) \times [(\langle n_{\mu} \rangle + 1) + \langle n_{\mu} \rangle] b\, d\Omega \quad , \quad (19)$$

where I_0 is the incident intensity, ρ is the density of the crystal, and b is the light pathlength through the medium. The index μ denotes the three acoustic branches (T_1, T_2, L) in the dispersion relation, and $\langle n_{\mu} \rangle = \{\exp[\hbar\Omega_{\mu}(\vec{K})/k_B T] - 1\}^{-1}$ is the mean occupation number of the phonons having a wave vector $\vec{K}$ and a polarization index μ. The two terms in the square brackets on the right-hand side of Eq. (19) correspond to the Stokes and anti-Stokes component. In a hexagonal crystal the direction of polarization of the light scattered from the mode μ is given by the vector[46]

$$\vec{\xi}^{\mu} = \hat{k}_{sc} \times \left\{ \hat{k}_{sc} \times \left[\frac{p_{44}}{\epsilon_{11}^2} [(\vec{\epsilon} \cdot \hat{\pi}^{\mu})(\hat{E}_0 \cdot \vec{\epsilon} \cdot \hat{\kappa}) + (\vec{\epsilon} \cdot \hat{\kappa})(\hat{E}_0 \cdot \vec{\epsilon} \cdot \hat{\pi}^{\mu})] - \frac{2p_{44}}{\epsilon_{11}^2} \sum_i \epsilon_{ii}^2 \pi_i^{\mu} \kappa_i E_{0,i} \vec{1}_i + \sum_m \left(\sum_i p_{mi} \frac{\epsilon_{mm}^2}{\epsilon_{11}^2} \pi_i^{\mu} \kappa_i \right) E_{0,m} \vec{1}_m \right.$$

$$\left. + \left(\frac{p_{11} - p_{12}}{2} - p_{44} \right) [(\pi_1^{\mu} \kappa_2 + \pi_2^{\mu} \kappa_1)(E_{0,2} \vec{1}_1 + E_{0,1} \vec{1}_2)] \right] \right\} \quad , \quad (20)$$

whose magnitude is $0 \le |\vec{\xi}^{\mu}| \le 1$. $\hat{\pi}^{\mu}$ is a unit vector in the direction of the polarization of the sound wave, $\hat{\kappa} = \vec{K}/K$ is a unit vector in the direction of the acoustic wave vector, $\hat{k}_{sc}$ is a unit vector in the direction of the scattered light, $\hat{E}_0$ is a unit vector in the direction of polarization of the incident light, and $\vec{1}_i (i = 1, 2, 3)$ are unit vectors along the cube axes. The components of $\hat{\pi}^{\mu}$, $\hat{\kappa}$, and $\hat{E}_0$ along the cube axes are π_i^{μ}, κ_i, and $E_{0,i}$. ϵ_{ii} $(i = 1, 2, 3)$ denotes the nonvanishing components of the relative dielectric constant tensor $(\vec{\epsilon})$ of the lattice in the absence of the elastic wave, and the p's are the appropriate photoelastic coefficients in contracted matrix notation.

For microwave acoustic phonons at room temperature one has $\hbar\Omega_{\mu}/k_B T \approx 10^{-3} - 10^{-5} \ll 1$ or, equivalently $\langle n_{\mu} \rangle \approx k_B T/\hbar\Omega_{\mu} \gg 1$, showing that the Stokes and anti-Stokes components are equal to intensity. Amplification of thermal lattice vibrations produces an increase in the occupation number (N_K^{μ}) above the equilibrium value $\langle n_{\mu} \rangle$. Thus, the corresponding anti-Stokes or Stokes scattering intensity for a certain acoustic mode can be written[46,50]

$$dI_{sc} = I_0 \frac{\pi^2 n_0^8}{\lambda_0^4} N_K^{\mu} \hbar\Omega_{\mu}(\vec{K}) \frac{|\vec{\xi}^{\mu}|^2}{2\rho V_{p,\mu}^2} b\, d\Omega \quad . \quad (21)$$

If the directional dependence of the factor $|\vec{\xi}^{\mu}|^2/V_{p,\mu}^2$ is known the scattering intensity yields information about the relative acoustic energy density in the modes $(\mu, \Omega_{\mu}, 0 \le \theta_p \le \frac{1}{2}\pi)$.

The derivation of Eq. (21) is based on the assumption that the attenuation of the incident light is negligible. In the present experiments the weak-scattering assumption is justified since it was observed that the depletion of the incident beam was always less than 1%. Thus, in contrast to the case of GaAs[13] the effect of multiple scattering, being important for intense scattering signals, is insignificant here.

In the scattering theory outlined above the scattering intensity has been calculated inside the medium. In a Brillouin-scattering experiment the intensity is measured outside the sample. A fixed aperture placed in front of the detector or the Fabray-Perot interferometer defines an external collection cone $d\Omega'$. For small-cone angles the rela-

tion between the collection cone inside and outside the crystal is

$$d\Omega = \frac{\cos^3\beta'}{\cos^3\beta}\,\frac{1}{n_a^2}\,d\Omega' \quad , \tag{22}$$

which varies as the sample and detector angles are changed.

The refraction and reflection corrections to the scattering intensity depend on both the polarization and propagation direction of the incident and scattered beam. The reflectivity of light polarized perpendicular ($R_\perp$) and parallel ($R_\parallel$) to the scattering plane is given by the Fresnel formula $R_\perp = \sin^2(u-u')/\sin^2(u+u')$ and $R_\parallel = \tan^2(u-u')/\tan^2(u+u')$, where $(u,\ u') = (\alpha,\ \alpha')$ or (β, β'). Taking into account multiple internal reflections of the scattered light the amount of scattered light transmitted through the backsurface becomes[37] $dI'_{sc} = dI_{sc}(1-R^i)/(1+R^d)$, where R^i and R^d are the reflectivities of the incident and scattered light, respectively. In a more detailed treatment one must consider also multiple internal reflections of the unscattered beam. In Fig. 9 is shown the reflectivity correction $(1-R^i)/(1+R^d)$ in ZnO and CdS for the scattering geometry of Fig. 7. The incident light is polarized parallel to the plane of incidence and it is assumed that the light undergoes a 90° rotation of polarization. It appears that the Fresnel corrections increase drastically with increasing "off-axis" angles of the phonons. The rapid drop at low acoustic frequencies is due to the birefringence, since the losses increase as we approach the collinear diffraction process.[51] At high frequencies the increase of the Bragg angle causes an increase in the Fresnel losses. Notice that the acoustic frequency range in which Brillouin scattering can occur decreases as the off-axis angle increases. An important implication of the above considerations is that the Stokes and anti-Stokes intensities in general are different outside the crystal. If the incident light were polarized perpendicular to the scattering plane the variations in the reflectivity correction would be qualitatively the same as sketched above. A comparison of the advantages and drawbacks of using a given polarization of the incident beam is considered elsewhere.[46]

As pointed out by Spears,[13] the angular dependence of the scattering intensity does not reflect the spectral distribution of the acoustic energy. From Eq. (21) we obtain the total scattering intensity from a number of acoustic modes in a small fixed volume of $\vec{k}$ space. According to the Debye theory, the number of acoustic modes per unit bandwidth is proportional to the square of the acoustic frequency f. The f^2 correction is only valid if the volume of $\vec{k}$ space probed by the light beam falls well within the cone of the amplified phonon beam.[13] If this is not the case, the frequency resolution and the angular resolution, especially for anisotropic crystal, can give rise to a more complicated conversion factor.

IV. EXPERIMENTAL RESULTS

A. Angular phonon distribution

Direct evidence for the idea that acoustoelectric domains in the longitudinal configuration consist

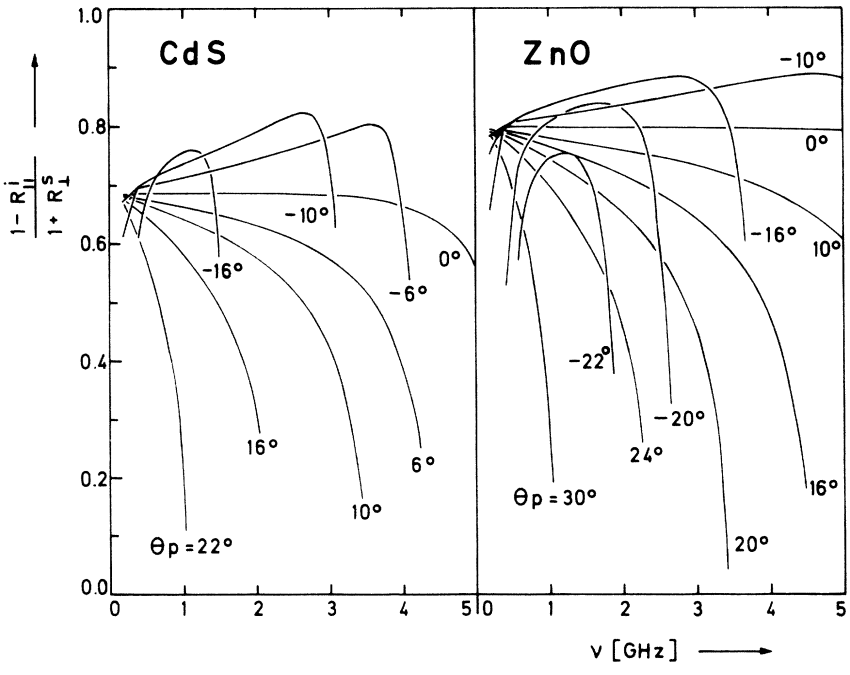

FIG. 9. Fresnel reflectivity correction as a function of acoustic frequency with θ_p as a parameter for the scattering geometry shown in Fig. 7.

of off-axis quasishear waves has been obtained by Brillouin scattering[14,52] and by studying the local change in birefringence induced by the strain accompanying the domains.[24]

In the following we shall discuss a Brillouin-scattering investigation of the angular phonon distribution in the strong-flux regime, i.e., at a stage where the phonon flux is sufficiently intense to give rise to significant nonlinear effects—among other things, current saturation.

As an example, we consider a semiconducting ZnO crystal with a length of 6.0 mm parallel to c and a hexagonal cross sectional area of 0.87 mm^2. The resistivity is $\rho \approx 7\ \Omega$cm and the mobility at 300 K is $\mu \approx 150$ cm^2/V sec. Applying high-voltage pulses, stable current saturation was observed above the threshold field $E_{th} \approx 1.8$ kV/cm. Superimposed on a spatial uniform flux, which caused the current saturation, a propagating domain was detected. After being destroyed in the anode contact, the domain was not replaced by a new one near the cathode. Continuous domain generation and current oscillations have been observed in only a few of the examined ZnO samples. From the measured domain velocity and from the polarization shift of the scattered light, which depends on the scattering geometry,[37] it is verified that the domains are composed of quasitransverse modes.

In Fig. 10 is shown the angular phonon distribution for various acoustic frequencies at a distance of 2.0 mm from the anode. The intensity of the scattered light is given in arbitrary units and has been corrected for reflection losses at the surfaces. The noise level is indicated in the lower part of the figure. It appears that the angular distribution has two maxima, and that the position of these (6°–8° from c) is independent of ω in the considered frequency range. This is plausible from linear theory. Since we have $\tilde{\omega}_c$, $\tilde{\omega}_D \gg \omega (0 \leq \theta_p \leq 90°)$ for frequencies in the range $0.6 \leq f < 2.4$ GHz the power amplification coefficient becomes $\beta_e = (K^2\tilde{\gamma}^2)/(V_p\tilde{\omega}_c)\omega^2$, showing that the angular dependence of the gain is independent of ω. Extending linear theory to the nonlinear region by simply making the drift parameter time dependent,[2,31] the above argument still holds. The maximum scattering intensity is obtained for a frequency $f_{mi} \approx 1.2$ GHz. If we include the ω^2 correction factor,[13] the frequency of maximum acoustic energy density equals 1.4 GHz, which is around a factor of 4 below the frequency of maximum linear net gain. The half-widths of the angular spectra are $\delta\theta_p \approx 8°$ for $f = 0.6$ or 2.2 GHz, $\delta\theta_p \approx 11°$ for $f = 1.2$ GHz, and $\delta\theta_p \approx 6°$ for $f = 2.4$ GHz. Linear theory predicts $\delta\theta_p = 2° - 4°$ in the considered frequency range. Thus nonlinear effects give rise to an appreciable broadening of the peaks, especially around f_{mi}. As the domain propagates $\delta\theta_p$ increases slightly and f_{mi} shifts continuously downward in accordance with other light-scattering experiments.[11,12,17,18]

The angular phonon distribution ($0 \leq \theta_p \leq 90°$) normally exhibits a single maximum, as shown in Fig. 10. However, in some of the investigated ZnO and CdS crystals two peaks were observed,

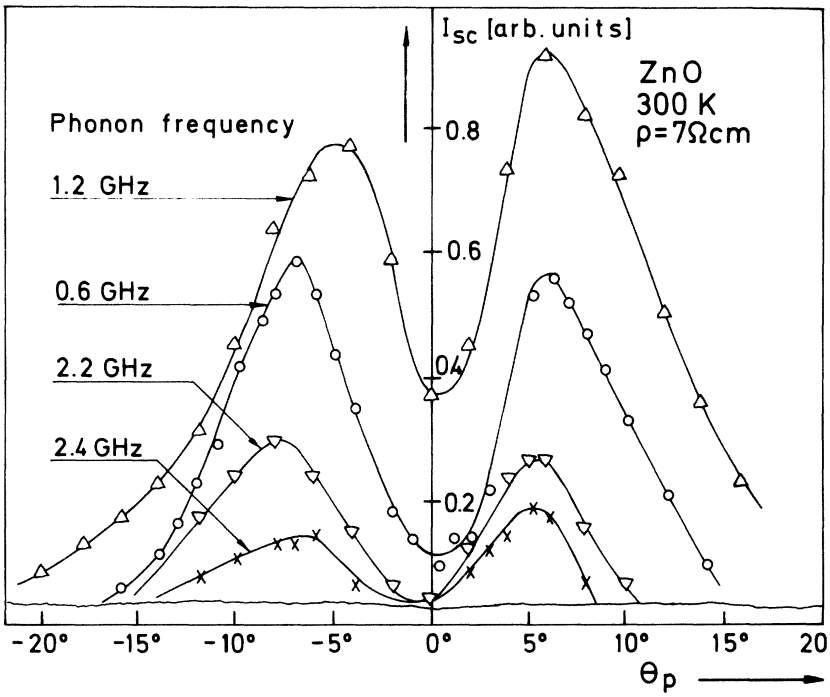

FIG. 10. Angular phonon distribution for different frequencies in the latest stage of flux growth.

but only in a certain frequency range and in the strong-flux regime. An angular distribution having two peaks is shown in Fig. 11. The normalized applied electric field was $E/E_{th} \approx 1.1$, and the sample resistivity $\rho \approx 5\ \Omega$cm. Two peak distributions were detected in the range ~0.6–2.0 GHz, at a distance of 2.0 mm from the anode (sample length parallel to c is 6.0 mm). At this stage of the flux growth a stationary spectrum with a maximum around $f_{mi} \approx 1.4$ GHz was attained. The two-peak structure is most pronounced for the highest frequency. One peak is localized at $\theta_p \approx 6°-7°$ and the other one at $\theta_p \approx 12°-14°$. In the linear regime only the peak at $\theta_p \approx 12°-14°$ is found. We suppose that the double peak should be ascribed to parametric down-conversion effects,[53,54] which are known to be significant in on-axis domains.[13]

Acoustic-wave dispersion does in general not allow phase-matched collinear three-phonon processes. To describe parametric effects in off-axis domains angular-dispersion effects must be taken into account. A theory doing this has not been published.

B. Off-axis angle of maximum intensity

Linear theory predicts that the off-axis angle of maximum gain for the phase propagation θ_{pm} increases monotonically with increasing electric field and tends to a constant value of about 30° for both ZnO and CdS (Fig. 2). However, waves propagating off the axis of the sample may suffer considerable loss because of diffuse scattering from the surfaces.[15,55] Such boundary scattering, introducing an additional nonelectronic loss, is thus expected to influence the angular distribution and the frequency distribution of the acoustic flux associated with off-axis domains, so that the off-axis angle of maximum intensity, θ_{pmi}, observed in the weak-flux region, not necessarily equals θ_{pm}.

Indirect experiments measuring the breakover point of non-Ohmic I-V characteristics seem to indicate that θ_{pmi} decreases as the sample cross section is reduced,[55] and that the sample aperture angle limits θ_{pmi}.[36]

Brillouin-scattering techniques make it possible to measure θ_{pmi} directly since we are able to analyze the individual plane-wave components of the domain. The influence of the cross section on θ_{pmi} has been studied in CdS crystals cut to rods having a length of 10 mm. The cross section varied from 0.5×0.5 mm^2 to 3.0×3.0 mm^2 and the samples had all a resistivity of $\rho \approx 16\ \Omega$cm. The selected frequency was equal to the frequency of maximum linear gain $f_m \approx 3.2$ GHz. For a cross section of 1.7×1.7 mm the saturation occurred at $\theta_{pmi} \approx 15°$, whereas the area 2.8×2.8 mm resulted in saturation at $\theta_{pmi} \approx 19°$.[14] The measurements were carried out at a fixed acoustic flux level. On a plot of current versus time, this corresponds to a fixed position with respect to the incubation time. Keeping a fixed flux level we obtain, so to speak, the same amount of nonlinearity in the domains. No simple relationship was found between the aperture angle and θ_{pmi}.[36]

In order to reduce geometric effects the measurements of θ_{pmi} were thus performed in a very broad CdS crystal. In Fig. 12 is shown θ_{pmi} as a function of the normalized drift velocity for an acoustic frequency of $f \approx f_m/4 \approx 800$ MHz. The measurements were carried out at a time just before the current starts to decay from its Ohmic value in order to keep the system linear, and the drift velocities were obtained from the Ohmic current.

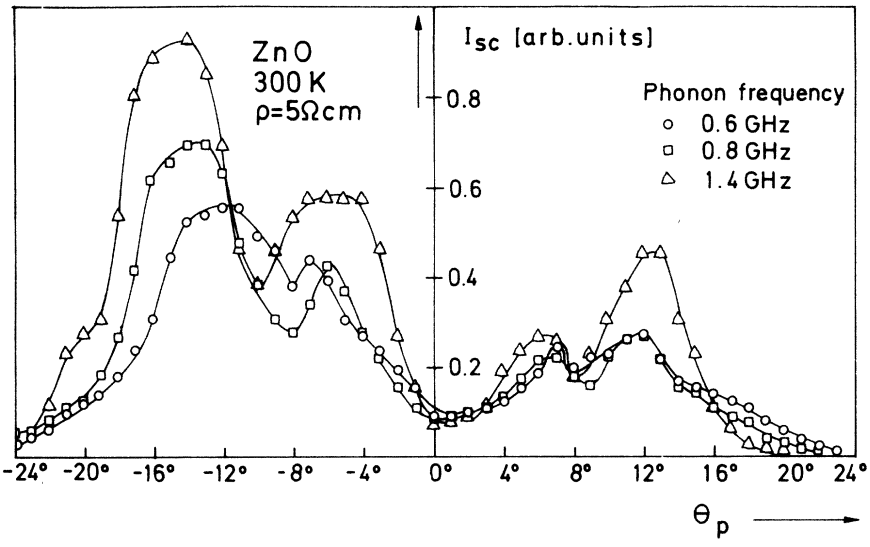

FIG. 11. Angular phonon distribution showing two-peak structure for different frequency components.

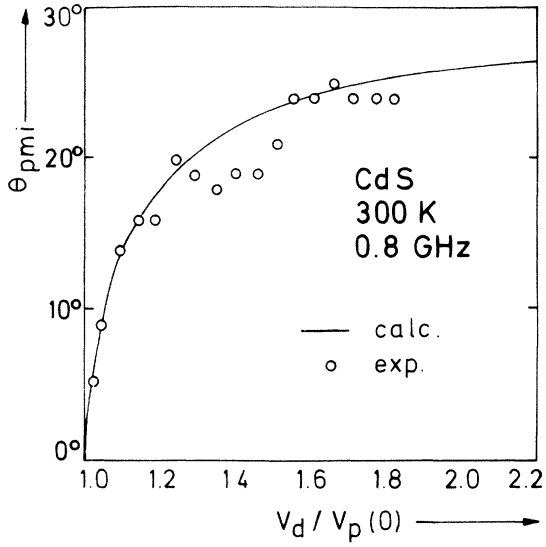

FIG. 12. Experimental results showing the off-axis angle of maximum intensity (θ_{pmi}) as a function of the normalized drift velocity at $\nu = 0.8$ GHz. The measurements were carried out at a time just before the current decay. The solid line represents the linear theory.

Under these conditions the over-all agreement with linear theory appears to be quite reasonable. For normalized drift velocities in the range $1.25 \leq V_d/V_p(0) \leq 1.5$ some discrepancy exists because of a saturation tendency at $\theta_{pm} \approx 18.5°$. At the moment, no explanation has been found for this intermediate saturation; only it should be noted that the data of Moore *et al.*[24] also show a saturation for $1.25 \leq V_d/V_p(0) \leq 1.5$. So far, we have not considered the influence of nonelectronic attenuation on θ_{pmi}. If the directional dependence of this loss mechanism is negligible, which it turns out to be in CdS,[38] the only effect of these losses is to cause a cutoff in θ_{pm} at electric fields close to the synchronous field.[37]

According to our discussion in Sec. II A, the free-carrier drift velocity falls towards a value close to the shear-wave phase velocity in the nonlinear region. This drop in $V_d(t)$ should be accompanied by a "track-down" in θ_{pm}. In order to examine this prediction we have followed the time development of θ_{pmi} before and after current saturation in a CdS sample ($10.0 \times 3.0 \times 1.0$ mm) exhibiting undamped current oscillations. The result for two acoustic frequencies is shown in Fig. 13. The normalized drift velocity calculated from the Ohmic current was $V_d/V_p(0) \approx 1.3-1.4$. According to Fig. 2, the corresponding off-axis angle of maximum linear gain should be $\theta_{pm} \approx 20°-22°$. The current starts to decay when the domain peak is 2.0 mm from the cathode. At this position we measure $\theta_{pmi} \approx 21°$, so that $\theta_{pmi} \approx \theta_{pm}$, as expected. During the current decay ($t \approx 0.3-0.4$ μ sec) the domain moves ~0.5–0.7 mm, and θ_{pmi} decreases linearly for both frequencies, the decay rate being somewhat larger for the high-frequency component, which is close to the frequency of maximum linear net gain f_{mn}. After complete current saturation, which is obtained when the domain is 2.7 mm from the cathode, the time dependence of θ_{pmi} becomes rather complicated. In a simplified description we could say that θ_{pmi} tends to decay towards $\theta_{pmi} \approx 14°-16°$, and that an oscillation of θ_{pmi}, especially for the low-frequency mode, is superimposed on this decay. The amplitude of the oscillation for the 1.6-GHz component is ~1.5°, and the distance between succeeding peaks of $\theta_{pm}(t)$ is 1–2 mm. This distance corresponds to an oscillation time $\tau \approx 0.6-1.1$ μ sec. Asdente *et al.*[56] have observed that the intensity of part of the frequency spectrum of the domain shows an oscillating character as a function of time. The period of these oscillations

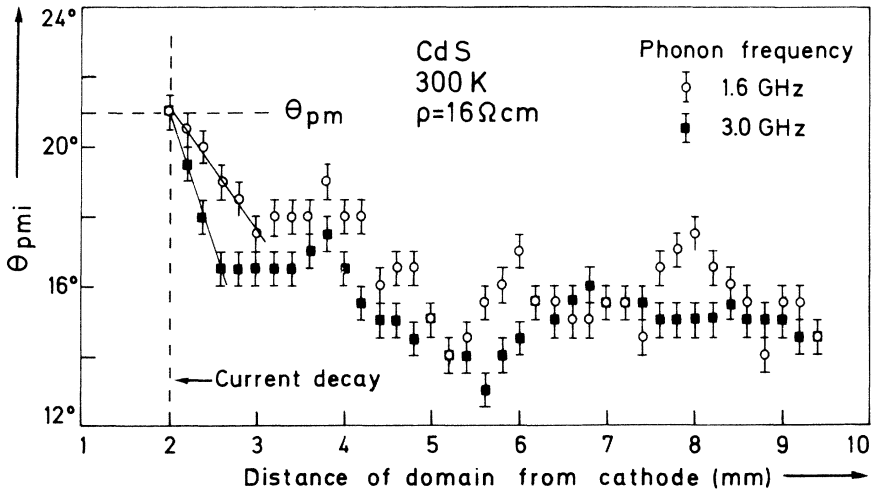

FIG. 13. Experimental results showing the off-axis angle of maximum intensity (θ_{pmi}) for two acoustic frequencies as a function of domain position. Note that oscillations in θ_{pmi} are superimposed on the "trackdown."

in a 2.2 – Ω cm CdS crystal is $\tau \sim 0.7$ μ sec, i.e., close to the period of our angular oscillations. It is plausible that parametric up and down conversion is responsible for these oscillations. Assuming a drift parameter, $\gamma(t) = V_d(t)\cos\theta_p / V_p(\theta_p) \rightarrow 1$, the saturation $\theta_{pmi} = 15^\circ$ yields $V_d / V_p(0) \approx 1.1$ at saturation.

C. Domain tilt angle

The previous part of Sec. IV has been concerned with the determination of the various aspects of off-axis acoustoelectric domains in an essentially one-dimensional model. In this section we shall deal with a two-dimensional picture of the off-axis domain as it is obtained by Brillouin scattering.

Using a strain-birefringent technique, Moore *et al.*[24] have been able to observe off-axis domains directly in CdS. The method which enables them to see the local concentration of the strain in some mean-square sense shows a straight domain inclined to the *c* axis. Measuring the domain tilt angle θ_D as a function of the initial electronic drift velocity they observe that $\theta_{pm} < \theta_D < \theta_{Em}$ for all drift velocities, where θ_{Em} is the off-axis angle of maximum gain for the energy propagating calculated on the basis of the acoustic-wave-dispersion theory outlined in Sec. II B. In their calculation only elastic angular dispersion was considered. This can be justified for two reasons. First, the acoustoelectric angular dispersion is quite small in CdS,[32] and second, most of the acoustic energy in the domain is concentrated in frequencies well below $\tilde{\omega}_m$.[11–14,17,18] Moore *et al.* claim that the discrepancy between theory and experiment is due to their inability to observe the acoustic flux in the linear region, and they suggest that the deviation of θ_D from θ_{Em} comes from a "track-down" of θ_{Em} as V_d falls towards V_p. Moore *et al.* assume *a priori* that θ_D equals θ_{Em}. This is not obvious if boundary conditions are imposed on the domain propagation.[15,55]

Furukawa *et al.*[57] have investigated off-axis domains by electrical probing on the sample surface and found a *V*-formed domain shape. Measuring the field dependence of θ_D for one of the branches they find $\theta_{pm} < \theta_D$. No comparison with θ_{Em} was made. Possible errors in their experiment arise again from the comparison of θ_D in the strong-flux regime with a linear model, and from the fact that potential probing, being confined to the crystal surface, may not give an accurate indication of the conditions within the bulk. Moreover, it is not obvious that one should directly compare the electrical and acoustical aspects of the domain.[58,59]

In the present section we shall examine the domain tilt angle in CdS, since this material is dominated by the simple frequency-independent elastic angular dispersion.

The spatial acoustic energy density associated with a plane-wave component is conveniently studied by Brillouin scattering. The scattering formula for optically anisotropic crystals enables one to select a given plane-wave component $(\nu, \vec{k})$, and the intensity of the scattered signal will be proportional to the acoustic energy density of the component in a broad frequency range.[37,51] By using Brillouin scattering as a two-dimensional optical probe we are in the position to study the domain tilt angle in detail.

The CdS crystals were cut to flat rods all having a length of 6–7 mm in the direction of the *c* axis. The cross section had the following values: 1.2×3.5, 1.2×6.0, and 1.2×8.0 mm. The resistivity was $\rho \approx 16$ Ω cm.

In Sec. III it was shown that θ_{pmi} varies as we change the applied voltage. Choosing the field to give $\theta_{pmi} \approx 20^\circ$ corresponding to $\theta_{Emi} \approx 37^\circ$ we obtain the maximum angular dispersion which is convenient for studying anisotropy effects.[32]

In Fig. 14 are shown the results obtained by two-dimensional optical probing of the off-axis domain. Two symmetric components $(f,\ \theta_p) \approx (1\ \text{GHz},\ \theta_{pmi} \approx \pm 20^\circ)$ were examined. It is seen that the spatial energy distribution of these modes has a characteristic *V* shape. Close to the cathode the acoustic mode $\theta_p = +20^\circ$ contributes to the energy density in the entire cross section. As the domain propagates the energy of the mode concentrates in the one of the branches, which tilt angle has the same sign as the considered off-axis angle for phase propagation. The energy distribution of the mode $\theta_p = -20^\circ$ is almost symmetric with that of $\theta_p = +20^\circ$ about a line parallel to the *c* axis in the middle of the sample. An investigation of different acoustic frequencies results in the same spatial distribution as discussed above. Thus the results indicate that the acoustoelectric domain in the present case is shaped as a *V* as long as we are not too near the cathode (see below). Each of the two straight domain branches mainly consists of plane-wave components with different frequencies having the same sign of the off-axis angle θ_p as the domain tilt angle θ_D. The width of the two branches is 200–300 μ. In some of our crystals having small cross sections, straight-shaped domains were observed.

It is evident from Fig. 14 that θ_D changes as the domain propagates along the sample. In Fig. 15 is shown the tilt angle as a function of time. The circles represent the longitudinal configuration. In the first stages of propagation θ_D increases linearly with time. After a period of ~ 1.8 μsec θ_D saturates at an angle close to 37°. Extrapolating the curve backwards in time the domain front should be perpendicular to the *c* axis near the cathode. A possible qualitative explanation of the shift

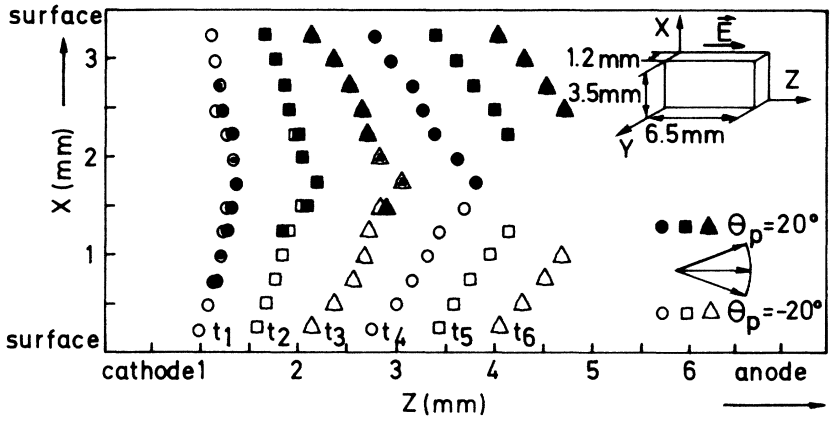

FIG. 14. Spatial distribution of peak acoustic intensity for the two plane-wave components (f_s, θ_p) = (1 GHz, ±20°) in acoustoelectric domain in CdS at 300 K. The energy distribution is plotted at the following times after onset of the voltage pulse: t_1, t_2, ..., t_6 = 0.4, 0.7, ..., 1.9 μsec. Crystal configuration: longitudinal. Full signatures correspond to $\theta_p = +20°$; open signatures correspond to $\theta_p = -20°$.

in θ_D as a function of time is as follows. Near the cathode the domain front is perpendicular to the c axis, indicating that the intensity of the $\vec{k}$-vector distribution must be symmetric around the rod axis over the entire cross section. This is plausible because the amplification coefficient is symmetric around c, and the "path lengths," along which the flux has been amplified, are equal for symmetric $\vec{k}$ vectors. This holds as long as we are in a region where the distance from the cathode is small compared to the sample dimension perpendicular to c. The extension of this region depends on the direction of the group velocity of the domain. Outside this region the acoustic flux coming from the lower part of the crystal, and moving in a direction given by $\vec{V}_g$, dominates in the upper part of the crystal, because of the difference in "path lengths" for acoustic flux moving in the direction $+\theta_E$ and $-\theta_E$. This gives rise to the tilt of the domain branches. This model is supported by the fact that we have observed an overlap region in the middle of the sample where both symmetric $\vec{k}$-vector distributions are present. Consequently, the domain obtains a boomeranglike shape. In the saturated region θ_D is determined by the total strain occurring from a $\vec{k}$-vector cone around the direction of maximum intensity. This agrees well with the observed saturation of the tilt angle at $\theta_D \approx 37°$ corresponding to the direction of energy propagation, θ_{Emi}, for the off-axis modes of maximum intensity $\theta_{pmi} \approx 20°$.

D. Domain splitting

In Sec. IVC we have treated the time and space development of the domain form without discussing how the acoustic energy is distributed in the two branches of the domain as it moves towards the anode.

In order to solve this problem Brillouin-scattering experiments were carried out along straight lines parallel to the c axis at different distances from the crystal boundary. The results for one of the branches are shown in Fig. 16. We have not on this plot tried to follow the acoustic flux back into the linear regime, but have only been interested in the well-established domain. The measurements were performed at fixed points in a coordinate system moving with the inclined V-formed domain. Since we investigate only one acoustic frequency, the intensity of the scattered light (in arbitrary units) gives directly the relative acoustic energy density of the mode in the considered space region.

It is evident that the energy distribution in the branch changes as a function of time. For a particular parameter value the acoustic peak intensity as a function of time has a maximum. Probing closer to the boundary this maximum is shifted towards the right, indicating that the acoustic wave packet moves outwards towards the surface. As time goes

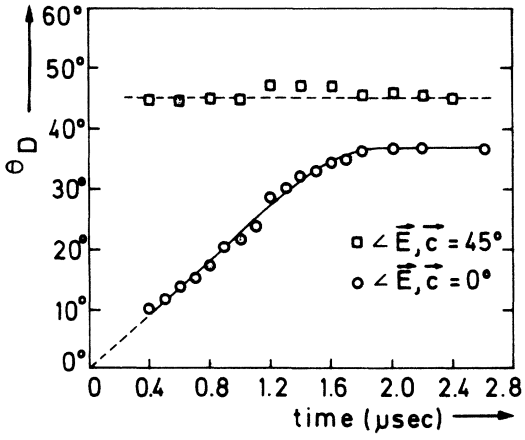

FIG. 15. Domain tilt angle (θ_D) in CdS at 300 K as a function of time measured from the onset of the electric field. Selected acoustic mode: (f_s, θ_p) = (1 GHz, 20°) for longitudinal configuration, and (f_s, θ_p) = (0.6 GHz, 33°) for 45° configuration.

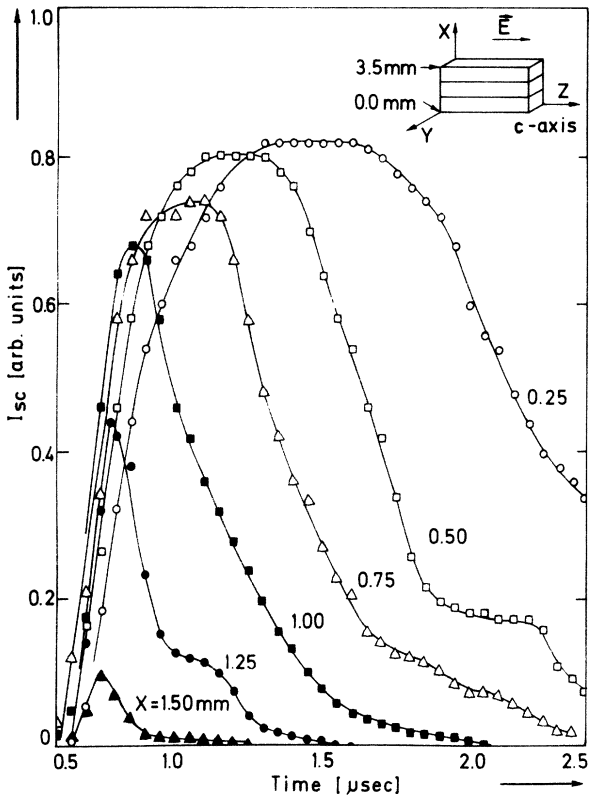

FIG. 16. Acoustic peak intensity as a function of time for the off-axis mode: $(f_s, \theta_p) = (1\ \text{GHz}, 20°)$ in acoustoelectric domain in CdS at 300 K. Configuration: longitudinal. Probing was performed along the c axis, and the parameter x gives the distance from the surface. Time is measured relative to the onset of the electric field.

on, the absolute value of the energy increases and shifts towards the crystal surface. After a certain time the acoustic energy density remains constant in two thin layers near the crystal surface for a relatively long time.

As the energy density increases near the surfaces, we observe an appreciable drop in the flux level in the center of the crystal, and finally the flux disappears completely, indicating that the V-formed domain has split up into two single domains propagating near the surfaces of the crystal. Thus, if the crystal has a circular cross section we would expect the domain to be annular. The net energy transport off the middle of the sample and the splitting of the flux indicate that the regeneration effect[24,34,60] in the central part of the crystal is rather incomplete.

E. Phonon focusing

A pronounced angular focusing of the acoustic flux with frequencies $\omega \ll \tilde{\omega}_m$ occurs around a direction 45° from the c axis in CdS.[14,32,42] Thus, wave vectors in the interval 30°–60° from c are focused in the energy cone $\theta_E \pm \Delta\theta_E = 45.3° \pm 0.9°$, and the relative spread in the group velocity component along the 45° direction $\Delta V_{s,45°}/V_{s,45°}$ is less than 1%. The $\vec{k}$-vector distribution in the 45° configuration (angle between applied electric field and c axis equals 45°) is in general not symmetric around the current direction. Linear theory predicts a shift with increasing electric field in the angle of maximum gain from ≈ 67°, corresponding to a direction where the electron-phonon coupling vanishes, to a saturation near 30°, where the electromechanical coupling constant has a maximum. Increasing the field the wave-vector cone changes its shape and the half-width grows. When the cone has a maximum at 45° it is very unsymmetric. In ZnO, on the other hand, the $\vec{k}$ vectors can be nearly symmetrically distributed around the field direction. This is due to the fact that K^2 has its maximum closer to the 45° direction and has a larger half-width in ZnO than in CdS. The half-width of the symmetric phase-velocity cone in

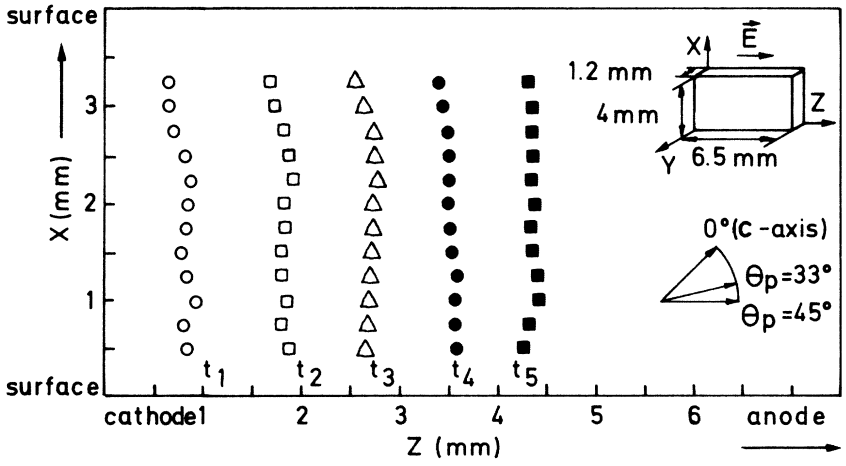

FIG. 17. Spatial distribution of peak acoustic energy in acoustoelectric domain as a function of time in 45° configuration. Investigated plane-wave component in CdS at 300 K: $(f_s, \theta_p) = (0.6\ \text{GHz}, 33°)$. The energy distribution is plotted at the following times after onset of the electric field: $t_1, t_2, \ldots, t_5 = 0.4, 0.8, \ldots, 2.0$ μsec.

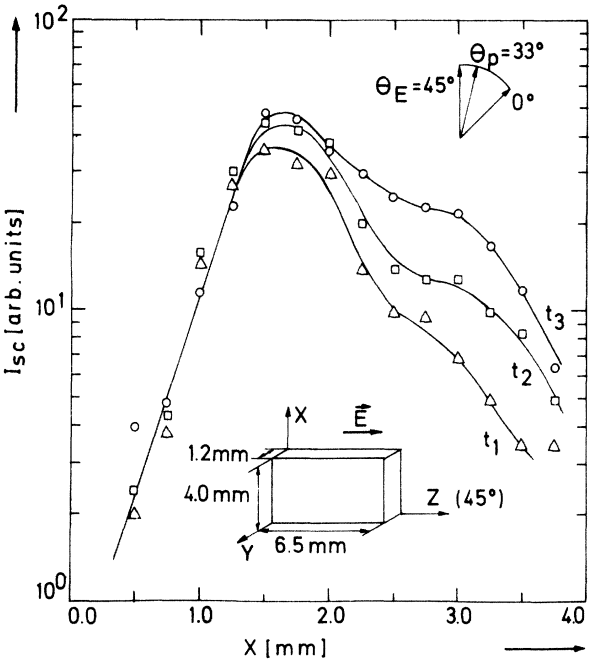

FIG. 18. Distribution of acoustic energy perpendicular to the current direction at different times ($t_1 = 0.4$, $t_2 = 0.6$, and $t_3 = 0.8$ μsec after onset of high-voltage pulse) in CdS at 300 K. Configuration: 45°. Investigated wave component: (f_s, θ_p) = (0.6 GHz, 33°).

ZnO is ~16° and the corresponding normalized field $E/E_{th} \approx 1.21$. A $\vec{k}$-vector distribution which is symmetric about the direction of the group velocity possesses a number of simple properties.

Experiments have been carried out on CdS crystals with dimensions 6.0×4.0×1.2 mm. The optic axis, which was placed in the 6.0×4.0 mm plane, formed an angle of 45° with the rod axis along which the electric field was applied.

The spatial distribution for a 600-MHz component of the acoustic flux at different times is shown in Fig. 17. The chosen off-axis angle of phase propagation equals 33°. It appears that the domain front is perpendicular to the rod axis, $\theta_D \approx 45°$, as expected because of the focusing effect.

The intensity distribution perpendicular to the current in the strong-flux regime at different times is shown in Fig. 18. In one part of the cross section, the flux level across the sample increases exponentially towards the middle of the sample but is time independent. In the other part a slight increase in intensity as a function of time is observed, and apparently some of the flux propagate outwards. In the 45° configuration acoustic modes with phase propagation at angles less than $\theta_p = 30°$ are present. These modes are not focused along the rod axis, and can give rise to the observed outward-propagating flux.

The difference between the domain form in the longitudinal and the 45° configuration is also reflected in the current. At the end of the domain transit the current returns to the Ohmic value. In the 45° configuration the domain collapses at the same time over the entire cross section, resulting in a rise time which is often a factor of 10 smaller than that associated with the tilted-domain destruction.[34] For the tilted domain the rise time is largest for broad samples, as expected.[34]

In a number of samples we have observed that the incubation time is about a factor of 2 smaller in the 45° configuration than in the longitudinal configuration.[34] This may be due to the smaller acoustic losses at the surface in the 45° configuration where energy is focused along the rod axis.

V. SOME REMARKS

A number of domain properties have been obtained by studying the frequency spectrum of on-axis domains. In the present work several new acoustical aspects of the propagating domain have been uncovered by investigating the angular phonon distribution and the two-dimensional properties of off-axis domains.

It is obvious that off-axis domains are especially suitable for studying anisotropy effects, and we believe that our knowledge of nonlinear effects can be improved considerably since these manifest themselves in both the frequency spectrum and the angular spectrum of the off-axis domains.

Although the complete process of domain growth and formation surely involves highly nonlinear interactions, our investigation has shown that linear theory leaves its imprint on the final domain structure.

ACKNOWLEDGMENTS

The author is indebted to Dr. E. Mosekilde for many stimulating discussions, and to Professor N. I. Meyer and Professor K. Maack Bisgård for their interest in the present work.

---

*Experimental part of this work included in a thesis in partial fulfillment of the requirements of the Ph. D. degree at The Technical University of Denmark, Lyngby, Denmark.

[1]A. R. Hutson and D. L. White, J. Appl. Phys. 33, 40 (1962).

[2]For an over-all description and extensive references see N. I. Meyer and M. H. Jørgensen [Adv. Solid State Phys. 10, 21 (1970)].

[3]A. Rose, RCA Rev. 27, 98 (1966); RCA Rev. 27, 600 (1966); RCA Rev. 28, 634 (1967); RCA Rev. 30, 435 (1969).

[4]H. N. Spector, Solid State Phys. 19, 291 (1966).
[5]P. O. Sliva and R. Bray, Phys. Rev. Lett. 14, 372 (1965).
[6]I. Yamashita, T. Ishiguro, and T. Tanaka, Japan J. Appl. Phys. 4, 470 (1965).
[7]W. Wettling and E. Pohlendt, Phys. Lett. 19, 268 (1965).
[8]W. H. Haydl and C. F. Quate, Phys. Lett. 20, 463 (1966).
[9]C. Hervouet, J. Lebailly, P. Leroux-Hugon, and R. Veilex, Solid State Commun. 3, 413 (1965).
[10]B. W. Hakki and S. Knight, Solid State Commun. 3, 89 (1965).
[11]J. Zucker, S. Zemon, and J. H. Wasko, in *II-VI Semiconducting Compounds*, edited by D. G. Thomas (Benjamin, New York, 1967).
[12]B. W. Hakki and R. W. Dixon, Appl. Phys. Lett. 14, 185 (1969).
[13]D. L. Spears, Phys. Rev. B 2, 1931 (1970).
[14]O. Keller, Phys. Status Solidi (a) 8, 61 (1971).
[15]M. Yamada, C. Hamaguchi, K. Matsumoto, and J. Nakai, Phys. Rev. B 7, 2682 (1973).
[16]J. Zucker and S. Zemon, Appl. Phys. Lett. 9, 398 (1966).
[17]A. Ishida and Y. Inuishi, Phys. Lett. 27A, 442 (1968).
[18]W. Wettling and M. Bruun, Phys. Status Solidi 34, 221 (1969).
[19]D. L. Spears, IBM J. Res. Develop. 13, 499 (1969).
[20]W. H. Haydl, K. Harker, and C. F. Quate, J. Appl. Phys. 38, 4295 (1967).
[21]W. H. Haydl and C. F. Quate, Appl. Phys. Lett. 7, 45 (1965).
[22]N. I. Meyer, M. H. Jørgensen, and I. Balslev, Solid State Commun. 3, 393 (1965).
[23]J. D. Maines, Appl. Phys. Lett. 8, 67 (1966).
[24]A. R. Moore, R. W. Smith, and P. Worcester, IBM J. Res. Develop. 13, 503 (1969).
[25]W. Wettling, Phys. Lett. 25A, 193 (1967).
[26]R. Bray, C. S. Kumar, J. B. Ross, and P. O. Sliva, J. Phys. Soc. Japan Suppl. 21, 487 (1966).
[27]H. Lemke, G. O. Müller, and E. Schnürer, Phys. Status Solidi 41, 539 (1970).
[28]T. Ishibashi, M. Kitamura, and A. Odajima, Phys. Lett. 44A, 371 (1973).
[29]A. Ishida and Y. Inuishi, J. Phys. Soc. Japan 26, 957 (1969).
[30]R. Klein, Phys. Lett. 28A, 428 (1968).
[31]R. K. L. Gay and H. L. Hartnagel, Phys. Status Solidi 30, 755 (1968).
[32]O. Keller, Phys. Status Solidi (a) 16, 87 (1973).
[33]M. Yamada, M. San'ya, C. Hamaguchi, and J. Nakai, Solid State Commun. 13, 483 (1973).
[34]O. Keller, Phys. Status Solidi (a) 10, 581 (1972).
[35]V. L. Gurevich, Fiz. Tverd. Tela 4, 909 (1962) [Sov. Phys.–Solid State 4, 668 (1962)].
[36]J. C. Huber, Appl. Phys. Lett. 16, 458 (1970).
[37]O. Keller, Ph. D. thesis (Technical University of Denmark, 1972) (unpublished).
[38]F. Siebert, O. Keller, and W. Wettling, Phys. Status Solidi (a) 4, 67 (1971).
[39]O. Keller, Phys. Lett. 39A, 235 (1972).
[40]E. Mosekilde, Ph. D. thesis (Technical University of Denmark, 1968) (unpublished).
[41]M. Born and K. Huang, *Dynamical Theory of Crystal Lattices* (Clarendon, Oxford, England, 1968).
[42]O. Keller, Solid State Commun. 13, 1541 (1973).
[43]C. F. Quate, C. D. W. Wilkinson, and D. K. Winslow, Proc. IEEE 53, 1604 (1965).
[44]R. W. Dixon, IEEE J. Quantum Electronics 3, 85 (1967).
[45]H. Küppers, Phys. Status Solidi 37, K59 (1970).
[46]O. Keller (unpublished).
[47]M. S. Kharusi and G. W. Farnell, Can. J. Phys. 47, 2719 (1969).
[48]G. Heiland, E. Mollwo, and F. Stöckmann, Solid State Phys. 8, 191 (1959).
[49]S. J. Czyzak, W. M. Bauker, R. C. Crane, and J. B. Howe, J. Opt. Soc. Am. 47, 240 (1957).
[50]G. B. Benedek and K. Fritsch, Phys. Rev. 149, 647 (1966).
[51]L. L. Hope, Phys. Rev. 166, 883 (1968).
[52]W. Wettling and M. Bruun, Phys. Lett. 27A, 123 (1968).
[53]E. A. Zabolotskaya, S. I. Soluyan, and R. H. Khokhlov, Acoust. Zh. 12, 188 (1966) [Sov. Phys.-Acoust. 12, 380 (1967).
[54]S. Zemon, J. Zucker, J. H. Wasko, E. M. Conwell, and A. K. Ganguly, Appl. Phys. Lett. 12, 378 (1968).
[55]J. H. McFee, P. K. Tien, and H. L. Hodges, J. Appl. Phys. 38, 1721 (1967).
[56]M. Asdente, J. Musci, and G. Ranclone, Phys. Lett. 33A, 475 (1970).
[57]S. Furukawa, T. Haka, and T. Motosugi, Appl. Phys. Lett. 16, 455 (1970).
[58]Y. Mita, J. Appl. Phys. 42, 2886 (1971).
[59]O. Keller, Phys. Lett. 43A, 65 (1973).
[60]M. Fukui and T. Arizumi, Japan J. Appl. Phys. 11, 634 (1972).